

Volatile static random access memory behavior of an aromatic polyimide bearing carbazole-tethered triphenylamine moieties

Lei Shi, Guofeng Tian, Hebo Ye, Shengli Qi*, Dezhen Wu

State Key Laboratory of Chemical Resource Engineering, Beijing University of Chemical Technology, Beijing 100029, China

ARTICLE INFO

Article history:

Received 13 August 2013

Received in revised form

16 December 2013

Accepted 23 December 2013

Available online 2 January 2014

Keywords:

Polyimide

Electrical memory

SRAM

ABSTRACT

A functional polyimide (6F/CzTPA PI), 4,4'-(hexafluoroisopropylidene)diphthalic anhydride (6FDA)/4,4'-diamino-4''-N-carbazolyltriphenylamine (DACzTPA), was synthesized in our present work for electrical resistive memory device applications. Semiconductor parameter analysis on the polyimide memory devices indicates that the synthesized polyimide possesses a volatile static random access memory (SRAM) characteristic with an ON/OFF current ratio of about 10^5 at the threshold voltage of around 1.5 V and -1.8 V. In addition, the device using the 6F/CzTPA PI as the active layer reveals excellent long-term operation stability with the endurance of reading cycles up to 10^8 under a voltage pulse and retention times for at least 8 h under constant voltage stress (-1 V). The charge transfer mechanisms and the roles of the donor and acceptor components in the PI macromolecules associated with the electrical switching effect are elucidated on the basis of the experimental and quantum simulation results.

© 2013 Elsevier Ltd. All rights reserved.

1. Introduction

In recent years, increasing attention has been paid to applications in memory devices based on polymeric materials possessing bistable electrical resistive switching effects [1–7]. As one of the most promising candidates for the next-generation memory devices characterized by the high data storage density, fast write/read speed, low power consumption and multilevel designs, such kind of polymer electronic materials possesses unique advantages, such as structural simplicity, good scalability, high mechanical flexibility, low fabrication cost, ease of processability, and three-dimensional (3D) multi-stacking capability for achieving high density data storage [8,9]. And completely different from that of the traditional silicon-based memory cells, which stores data by encoding each device as “0” or “1”, polymer memory achieves information storage based on the bistability of the materials, for instance, the high and low electrical conductivity response to an applied voltage [10].

Many polymeric materials have been explored and some of them have been demonstrated to exhibit excellent electrical resistive switching effects with potentials to be applied in memory devices, including conjugated polymers such as poly(9,9-bis(4-diphenylaminophenyl)-2,7-fluorene) (PDPAF) [11], vinyl polymers with specific pendent groups such as poly(N-vinylcarbazole) (PVK) [12–15], functional polyimides (PIs) [16–19], and polymer

nanocomposites embedded with metal nanoparticles (NPs) [20–22], fullerenes [23–25], carbon nanotubes (CNTs) [26,27], grapheme [28], and graphene oxide (GO) [29]. Among them, aromatic PIs have gained most widespread attentions in recent years due to their excellent thermal and mechanical properties, high-temperature dimensional stability, chemical inertness, and good processability [30]. These functional electroactive PIs were usually designed to contain both electron-donating and electron-accepting groups within a repeating unit, which can contribute to electronic transitions between the ground and excited states through the induced charge transfer between the electron donor (D) and acceptor (A) moieties under applied electric fields, and therefore exhibit electrical memory behaviors [31–33]. By introducing different electron donor and acceptor moieties into the polymer chain or by designing different molecular structures, PIs have been demonstrated to be able to exhibit non-volatile or volatile memory effect [30,34–37]. This makes us believe that by combining suitable functional groups into the polyimide chain through elaborate molecular design, it is possible to finely tune the highest occupied molecular orbital (HOMO) energy level, the lowest unoccupied molecular orbital (LUMO) energy level, the dipole moment as well as the charge transport ability of the synthesized polyimides and consequently lead to novel electrical memory effect [38–40].

Herein, we report our works on the synthesis and electrical characterization of an aromatic polyimide, 4,4'-(hexafluoroisopropylidene)diphthalic anhydride/4,4'-diamino-4''-N-carbazolyltriphenylamine (6F/CzTPA PI), with structures in which the carbazole-tethered triphenylamine units (CzTPA) function as the

* Corresponding author.

E-mail address: qisl@mail.buct.edu.cn (S. Qi).

electron-donating moieties and the hexafluoroisopropylidene phthalimide units (6FDA) serve as the electron-accepting species. Both triphenylamine (TPA) and carbazole (Cz) are typical electron-donating groups, and previous researches by combining them individually with electron acceptor groups have revealed soluble electroactive polyimides showing different memory behaviors such as dynamic random access memory (DRAM) [5,8,36,41–46] and static random access memory (SRAM) [35,36,45] behaviors. Here, the integration of the TPA unit and the Cz unit to form the CzTPA moiety and its subsequent utilization as the electron-donating species is supposed to be able to enhance the electron donating and charge transport capabilities of the resulting polyimide, and correspondingly endow the synthesized material with stronger potential to form electron donor–acceptor couples and consequently novel memory effect. Electrical characterization results suggest that the polymer possesses electrical bistability and the memory devices using the synthesized polyimide as the active layer (ITO/Thin 6F/CzTPA PI Layer/Au) exhibit volatile electrical switching effect, which could be swept both positively and negatively from the low-conductivity (OFF) state to the high-conductivity (ON) state with an ON/OFF current ratio of about 10^5 and a switching time less than 20 ns, and could be applied as static random access memory (SRAM) in digital information storage. Theoretical model analysis was carried out to elucidate the electrical conducting process occurring in the synthesized polyimide. Molecular simulation of the 6F/CzTPA model compound was conducted to clarify the carrier transport process and memory mechanisms in the electroactive polyimide.

2. Experimental

2.1. Materials

4-Fluoronitrobenzene, carbazole, hydrazine monohydrate, 10% palladium on activated carbon (10% Pd/C), isoquinoline, and cesium fluoride were purchased from J&K Scientific Co. Ltd. Anhydrous potassium carbonate, anhydrous magnesium sulfate, sodium hydroxide (NaOH), tin(II) chloride dihydrate, 1-methyl-2-pyrrolidinone (NMP), dimethylacetamide (DMAc), dimethylformamide (DMF), tetrahydrofuran (THF), ethyl acetate, toluene, chloroform, acetone, isopropanol, methanol and ethanol were purchased from Beijing Chemical Works, and they were all used as received. m-Cresol was also bought from Beijing Chemical Works, and it was purified by distillation over zinc powder and stored over 4 Å molecular sieves prior to use. The 4,4'-(hexafluoroisopropylidene) diphthalic anhydride (6FDA) was obtained from Sigma–Aldrich (Shanghai) Trading Co. and sublimated before use.

2.2. Characterization

Fourier transform infrared (FT-IR) spectra were recorded under ambient conditions on a Bruker Tensor 27 Fourier transform spectrophotometer. KBr was used as a nonabsorbent medium. Proton nuclear magnetic resonance (^1H NMR, 400 MHz) spectra were recorded on a Bruker AV400 spectrometer using DMSO- d_6 and CDCl_3 as the solvent. Differential scanning calorimetry (DSC) measurements were performed on a TA Q20 system at a heating rate of $10\text{ }^\circ\text{C min}^{-1}$ under nitrogen atmospheres. Thermogravimetric analysis (TGA) was undertaken under nitrogen atmospheres using a TA Q50 instrument at a heating rate of $10\text{ }^\circ\text{C min}^{-1}$. Gel permeation chromatography (GPC) analysis was carried out on a Waters 515-2410 system using polystyrene standard as the molecular weight reference and THF as the eluent. Ultraviolet–visible (UV/vis) absorption spectra were recorded on a Shimadzu UV-2550 spectrophotometer. Cyclic voltammetry (CV) measurement was

performed on a CHI660D Electrochemical Workstation (Shanghai Chenhua Instruments Inc., China) using a three-electrode cell under nitrogen environment. The polyimide films coated on a platinum square electrode (working electrode) were scanned anodically and cathodically (scan rate: 100 mV s^{-1}) in a solution of tetrabutylammonium tetrafluoroborate ($n\text{-Bu}_4\text{BF}_4$) in dry acetonitrile (0.1 M) with Ag/AgCl and a platinum net as the reference electrode and auxiliary electrode, respectively. Ferrocene was used as the external reference for calibration (0.38 V vs. Ag/AgCl). The thickness of the polyimide films coated on the ITO substrate was measured using atomic force microscopy (Digital Instruments Nanoscope IIIa, Veeco Instrument) under contact mode. The current–voltage (I – V) characteristics of the sandwich devices were recorded by a Keithley 4200 SCS semiconductor parameter analyzer equipped with a Micromanipulator PW-600 probe station (Advanced Technology Co., limited, Hong Kong) in a clean and metallic shielding box in ambient environment at room temperature. Molecular simulations were carried out on the basic unit of the synthesized polyimide using the Gaussian 09 program package. The molecular orbitals and electronic properties were calculated on theory levels including semi-empirical, ab initio and density functional theory (DFT).

2.3. Monomer synthesis and polyimide synthesis

Scheme 1 shows the synthetic route for the DACzTPA diamine monomer and the final 6F/CzTPA polyimide. Details on their preparation and characterization are given below. The 4,4'-diamino-4''-N-carbazolyltriphenylamine (DACzTPA) was synthesized by the condensation of N-(4-aminophenyl)carbazole (APCB) with 4-fluoronitrobenzene in the presence of cesium fluoride, followed by the hydrazine monohydrate Pd/C-catalyzed reduction of the intermediated dinitro compound (DNCzTPA) according to a similar procedure reported previously [47].

2.3.1. Synthesis of N-(4-nitrophenyl)carbazole (NPCB)

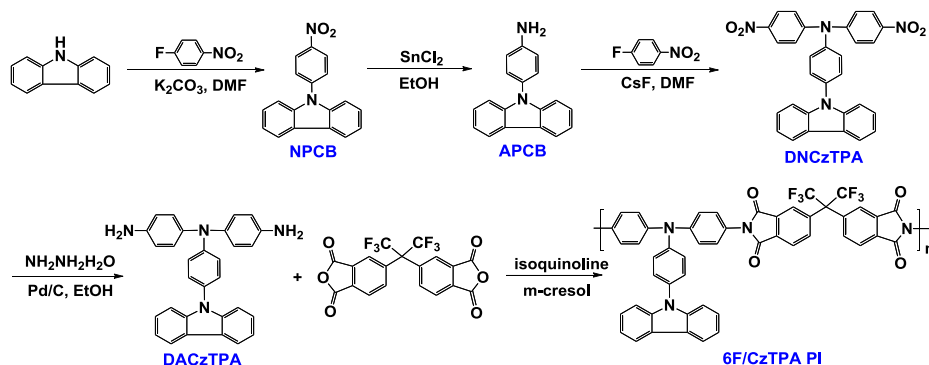
To a solution of 8.36 g (0.05 mol) of carbazole and 5.3 ml (0.05 mol) of 4-fluoronitrobenzene in 100 ml of DMF, 4.14 g (0.03 mol) of anhydrous potassium carbonate was added with stirring at one portion. After heating at $150\text{ }^\circ\text{C}$ for 15 h under nitrogen atmosphere, the mixture was poured into 800 ml of distilled water under stirring to obtain a yellow precipitate. The crude product was then collected by filtration and recrystallized with ethyl acetate to afford 11.5 g (80% in yield) of yellow crystals. DSC: m.p. $211\text{ }^\circ\text{C}$ and FT-IR (KBr, cm^{-1}): 1594, 1344 (NO_2 stretch). ^1H NMR (DMSO- d_6 , 400 MHz), δ (ppm): 8.50 (d, 2H, $J = 9.04\text{ Hz}$), 8.28 (d, 2H, $J = 7.53\text{ Hz}$), 7.98 (d, 2H, $J = 9.05\text{ Hz}$), 7.56 (d, 2H, $J = 8.24\text{ Hz}$), 7.49 (t, 2H, $J = 7.70\text{ Hz}$), 7.36 (t, 2H, $J = 7.86\text{ Hz}$).

2.3.2. Synthesis of N-(4-aminophenyl)carbazole (APCB)

To a solution of 5.76 g (0.02 mol) of NPCB in 40 ml ethanol, 15.8 g (0.07 mol) of $\text{SnCl}_2 \cdot 2\text{H}_2\text{O}$ was added. After refluxing for 24 h, the reaction mixture was condensed under reduced pressure to distill off most of the ethanol followed by neutralization with 40 wt% aqueous NaOH solution until the mixture became alkaline. The resulting mixture was then extracted with toluene, dried over anhydrous magnesium sulfate, and evaporated under reduced pressure to get 4.5 g (85% in yield) of yellowish syrup. FT-IR (KBr, cm^{-1}): 3375, 3459 (N–H stretch). ^1H NMR (DMSO- d_6 , 400 MHz), δ (ppm): 8.19 (d, 2H, $J = 7.67\text{ Hz}$), 7.40 (t, 2H, $J = 7.66\text{ Hz}$), 7.26–7.17 (m, 6H), 6.79 (d, 2H, $J = 8.61\text{ Hz}$), 5.43 (s, 2H).

2.3.3. Synthesis of 4,4'-dinitro-4''-N-carbazolyltriphenylamine (DNCzTPA)

To a solution of 2.58 g (10 mmol) of APCB and 2.2 ml (21 mmol) of 4-fluoronitrobenzene in 50 ml of DMF, 1.52 g (10 mmol) of



Scheme 1. Synthetic route for the DACzTPA monomer and the 6F/CzTPA polyimide.

cesium fluoride was added with stirring at one portion, and then heated at 150 °C for 24 h under nitrogen atmosphere. The resulting mixture was then poured into 500 ml of methanol to yield a yellow precipitate followed by filtration, washing thoroughly by ethanol and drying in vacuum to afford 3.75 g (75% in yield) of yellow solid. DSC: m.p. 296 °C and FT-IR (KBr, cm^{-1}): 1579, 1308 (NO_2 stretch). ^1H NMR (DMSO-d_6 , 400 MHz), δ (ppm): 8.28~8.25 (m, 6H), 7.75 (d, 2H, $J = 8.61$ Hz), 7.53 (d, 2H, $J = 8.59$ Hz), 7.53~7.46 (m, 4H), 7.36 (d, 4H, $J = 9.14$ Hz), 7.32 (t, 2H, $J = 7.82$ Hz).

2.3.4. Synthesis of 4,4'-diamino-4''-N-carbazolyltriphenylamine (DACzTPA)

In a 100 ml round-bottom flask equipped with magnetic stirring, 1.00 g (2 mmol) DNCzTPA and 0.3 g of 10% Pd/C were dissolved/suspended in 30 ml of ethanol. The suspension solution was then heated to reflux for 24 h under the dropwise addition of 5 ml hydrazine monohydrate (finish in 2 h), followed by hot filtration to remove the Pd/C, recrystallization from ethanol and drying in vacuum at 50 °C overnight to yield 0.70 g (80% in yield) of light-purple crystals. DSC: m.p. 194 °C and FT-IR (KBr, cm^{-1}): 3371, 3232 (N–H stretch). ^1H NMR (DMSO-d_6 , 400 MHz), δ (ppm): 8.20 (d, 2H, $J = 7.70$ Hz), 7.41 (t, 2H, $J = 8.19$ Hz), 7.30 (d, 2H, $J = 8.18$ Hz), 7.27~7.23 (m, 4H), 6.97 (d, 2H, $J = 8.63$ Hz), 6.78 (d, 2H, $J = 8.92$ Hz), 6.60 (d, 2H, $J = 8.65$ Hz), 5.06 (s, 2H).

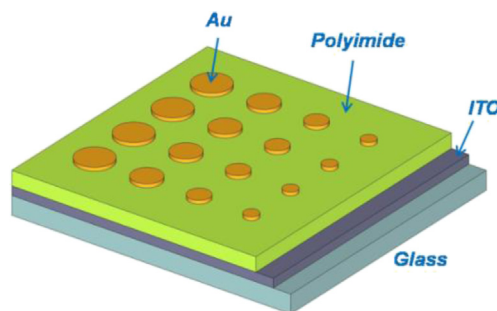
2.3.5. Synthesis of the 6F/CzTPA polyimide

The 6F/CzTPA PI was synthesized from diamine DACzTPA and dianhydride 6FDA by the conventional one-step method. To a solution of 0.440 g (1 mmol) of DACzTPA in 8 ml of m-cresol, 0.444 g (1 mmol) of 6FDA and 2 ml of isoquinoline were added in one portion. The mixture was stirred for 2 h at ambient temperature under N_2 atmosphere and then heated to 190 °C and maintained at that temperature for 12 h. After cooling down to ambient temperature, the viscous solution was poured slowly into 400 ml of methanol with stirring to yield the polyimide as a precipitate. The crude product was then collected by filtration, washed thoroughly with hot methanol, and dried at 120 °C overnight to give the final polyimide (0.76 g, 86% in yield). FT-IR (KBr, cm^{-1}): 1784, 1725, 1370, 723 (imide ring) (see Fig. S1 for the IR spectrum). ^1H NMR (CDCl_3 , 400 MHz), δ (ppm): 8.12 (d, 2H, $J = 7.82$ Hz), 8.04 (d, 2H, $J = 7.98$ Hz), 7.96 (s, 2H), 7.87 (d, 2H, $J = 7.73$ Hz), 7.51~7.27 (m, 18H) (see Fig. S2 for the ^1H NMR spectrum). The 6F/CzTPA PI exhibits good solubility in common solvents, such as chloroform, THF, DMF, DMAc, and NMP, at room temperature, due to the bulkiness and low surface energy of the trifluoromethyl group in 6FDA. It can be cast into transparent and uniform films from solutions by spin coating. The inherent viscosity of the resulting polyimide was 0.73 dL g^{-1} , measured in DMAc at a concentration of 0.5 g dL^{-1} at 30 °C. The

number average molecular weight (M_n) and the weight average molecular weight (M_w) of the polymer are $4.6 \times 10^4 \text{ g mol}^{-1}$ and $8.7 \times 10^4 \text{ g mol}^{-1}$, respectively, with the polydispersity index of 1.9, as determined by GPC (polystyrene as standard, THF as solvent and eluent). In addition, as evaluated by TGA and DSC measurements, the 6F/CzTPA PI not only exhibits excellent thermal stability with the 5% and 10% weight loss temperatures up to 510 °C and 557 °C (see Fig. S3 for the TGA curve), but also possesses a high glass transition temperature (T_g) of about 327 °C (see Fig. S4 for the DSC curve).

2.4. Sandwich memory device fabrication

The sandwich memory devices using the synthesized 6F/CzTPA PI as the active layer were fabricated by spreading a 20 mg ml^{-1} polyimide solution in DMAc onto a precleaned indium-tin oxide (ITO) substrate using a spin coater set at 1500 rpm for 40 s. The ITO conductive glass was precleaned sequentially with water, acetone, chloroform and isopropanol by ultrasonication for 15 min and then dried by a N_2 gun. After keeping in a clean box programmed at constant temperature and humidity for ca. 4 h, the spin-coated polyimide films were then baked at 100 °C for 5 h under vacuum to remove the residual solvent. ^1H NMR measurement was carried out to confirm that the solvent (i.e., DMAc) was completely removed from the active layer. The thickness of the polyimide films coated on ITO was around 50 nm, as determined by atomic force microscopy measurement. Finally, the sandwich devices were fabricated by vacuum evaporation of a thin Au layer with the thickness of ca. 100 nm through a shadow mask onto the polymer surface as the top electrode, the structure of which is shown in Scheme 2. The sandwich memory devices were eventually prepared with the configuration of ITO/Thin 6F/CzTPA PI Layer/Au.



Scheme 2. Illustrative structures for the ITO/Thin 6F/CzTPA PI Layer/Au sandwich device.

3. Results and discussion

3.1. Optical and electrochemical properties of the 6F/CzTPA polyimide

Fig. 1(a) shows the UV/vis absorption spectrum for the synthesized 6F/CzTPA PI, as well as the 6FDA and DACzTPA monomers in THF. A distinct absorbance band centered at around 326 nm (λ_{max}) was observed on the spectrum of the 6F/CzTPA PI, with the absorption edge extending to a wavelength (λ_{edge}) of 372 nm, based on which the optical energy band gap (E_g) of the material was calculated to be 3.33 eV according to the Plank equation ($E_g = hc/\lambda_{\text{edge}}$). This strong UV absorption peak was supposed to be ascribed to the $n-\pi^*$ transitions resulting from the conjugation between the aromatic rings and nitrogen atoms that combine the characteristic $\pi-\pi^*$ transitions of triphenylamine and carbazole groups. Here, the electron-withdrawing 6FDA species is believed to have promoted the delocalization and conjugation of the current $n-\pi$ and $\pi-\pi$ electronic system, since the UV/vis spectra in Fig. 1(a) indicate that the absorption of the 6F/CzTPA PI at 326 nm was obviously enhanced as compared to the individual CzTPA monomer.

The electrochemical behavior of the synthesized polyimide was investigated by cyclic voltammetry (CV) measurements conducted using the thin PI film cast on a pre-cleaned square platinum plate as the working electrode to elucidate the relative ionization and reduction potentials of our electroactive materials. Fig. 1(b) shows the CV sweeps for both the p-doping and n-doping processes for the synthesized 6F/CzTPA polyimide on platinum in the potential range of -2.0 to $+2.0$ V. The CV curve indicates that the 6F/CzTPA polyimide exhibits a quasi-reversible p-doping behavior during the anodical scan from 0 to $+2.0$ V. A strong ionization (oxidation) peak was observed at around 1.71 V (vs. Ag/AgCl electrode), whereas two reduction peaks appear at about 1.14 V (weak) and 0.81 V (moderate) when scanning backward. The results imply that the CzTPA units consisted of carbazole and triphenylamine in the 6F/CzTPA polyimide have a strong tendency to donate electrons and, as expected, readily function as hole-transporting sites in the material. This is under expectation since carbazole and triphenylamine are typical electron-donating moieties, and both of them have been demonstrated to possess the ability to enhance the hole-injection properties when being introduced into a material [46,48].

When scanning cathodically from 0 to -2 V, the polymer film exhibits a distinct reduction peak at about -1.40 V (vs. Ag/AgCl electrode), which is supposed to be related to the electrochemical reduction of the 6FDA units that have a high tendency to adopt electrons. However, the CV result indicates that this n-doping process is also quasi-reversible, as verified by the observation of two oxidation peaks at about -0.96 V (weak) and -0.33 V

(moderate) when scanning backward. Nevertheless, the predominant reduction peak at -1.40 V demonstrates the strong electron-withdrawing ability of the 6FDA units. Besides, the polyimide exhibits good CV reversibility during repeated cyclic scans between -2.0 V and $+2.0$ V, indicating the excellent electrochemical stability of the synthesized polyimide and the good adhesion at the polymer-platinum interface. The quasi-reversible electron-donating and electron-accepting behaviors observed here are suggested to be partially responsible for the quasi-reversible (delayed relaxation) electrical switching effect observed in the sandwich memory devices shown later.

In addition, the energy levels of HOMO (the top of the valence band) and LUMO (the bottom of the conduction band) of the synthesized polyimide can be quantitatively calculated from the CV onset oxidation potential ($E_{\text{ox}}(\text{onset})$) and the energy band gap (E_g) obtained from the UV/vis absorption spectrum according to the following equations: [41,49,50]

$$\text{HOMO} = -[(E_{\text{ox}}(\text{onset}) - E_{\text{ferrocene}}) + 4.8] (\text{eV}) \quad (1)$$

$$\text{LUMO} = E_g + \text{HOMO} \quad (2)$$

where $E_{\text{ferrocene}}$ is the potential of the external standard, ferrocene–ferrocenium (Fc/Fc^+), which is determined to be 0.38 V vs. Ag/AgCl under the same CV measurement conditions for the 6F/CzTPA PI. The absolute energy level of ferrocene is 4.8 eV below the vacuum level (i.e., 0 eV), and was used as the calibration reference.

As determined from the CV curve, the $E_{\text{ox}}(\text{onset})$ for the polyimide is at around 0.89 V vs. Ag/AgCl, and as calculated previously from the UV/vis absorption edge wavelength, the energy band gap (E_g) is 3.33 eV. Thus, the HOMO and LUMO energy levels of the 6F/CzTPA polyimide are estimated to be -5.31 and -1.98 eV, respectively. In comparison, the onset reduction potential ($E_{\text{red}}(\text{onset})$) of the polyimide determined from the CV sweeps was -1.00 V, giving a CV energy band gap of 1.89 eV, which deviates significantly from the optical band gap (3.33 eV) estimated from the UV/vis absorption spectrum, which is common and often encountered in literatures.

3.2. Memory effects and device performance

The electrical switching effect of the synthesized PI was demonstrated by the current–voltage (I – V) characteristics of the Au|polyimide|ITO sandwich devices, as shown in Fig. 2(a). During the first positive scan from 0 to 3 V (with ITO as cathode and Au as anode), a progressive increase in the current occurring at a threshold voltage of around 1.5 V was observed, indicating the

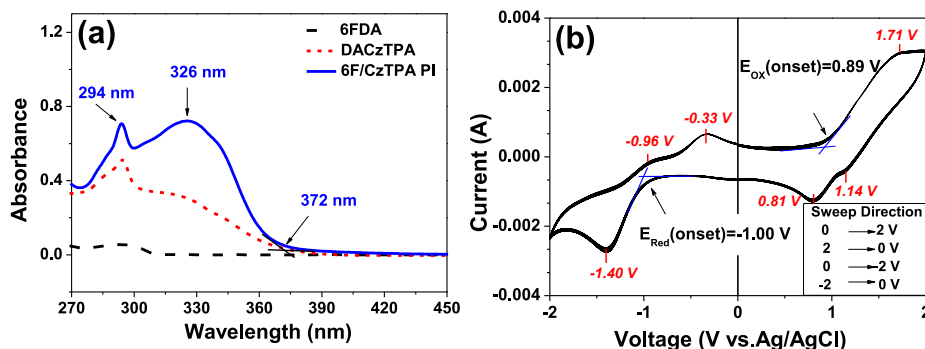


Fig. 1. (a) UV/vis absorption spectrum of 6FDA, DACzTPA and 6F/CzTPA PI. (b) Cyclic voltammetry sweeps of the 6F/CzTPA PI measured in 0.1 M $n\text{-Bu}_4\text{BF}_4/\text{acetonitrile}$ (scan rate: 100 mV s^{-1}).

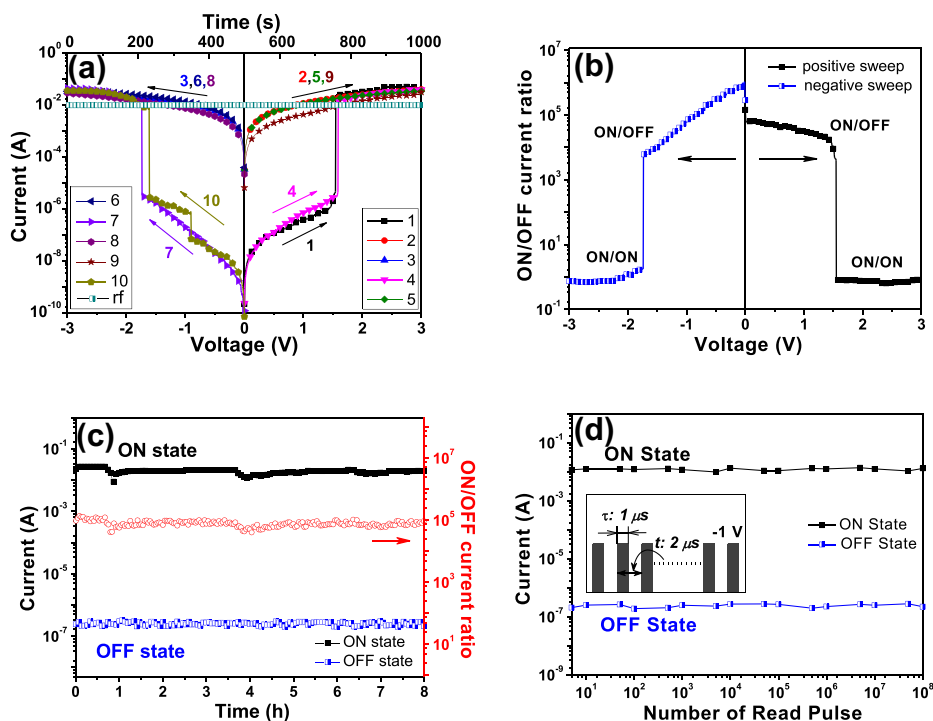


Fig. 2. (a) Current–voltage (I – V) characteristics of the ITO/Thin 6F/CzTPA PI Layer/Au sandwich device; the sweep sequence and direction are indicated by the number and arrow. The fourth, seventh and the tenth sweeps were conducted about 10 min after turning off the power. The ON state was sustained by a refreshing voltage pulse of -1 V (pulse duration = 1 ms) in every 5 s, as shown by the “rf” trace. (b) The ON- to OFF-state current ratios for both positive and negative sweeps as a function of applied voltage. (c) Effect of operation time on the currents of the sandwich device at the ON and OFF states tested at -1 V bias under ambient conditions. (d) Effect of -1 V read pulse on the ON and OFF states of the sandwich device. The inset shows the pulse shapes in the measurement (2 μ s in period, 1 μ s in duration width).

transition of the sandwich device from the low-conductivity state (the OFF state) to the high-conductivity state (the ON state). The ratio of the conductivities achieved between the two states is at around 10^5 . After this transition, the device remained in the high-conductivity state, as observed during the following positive scan (the second sweep). And the subsequent negative scan from 0 to -3 V (the third sweep) did not turn the device from the ON state to the OFF state, indicating that the memory device cannot be retrieved to the initial OFF state by applying a reverse bias sweep, and therefore is “unerasable”. However, the electrical characterization results indicate that the ON state of the device could only be retained temporarily, and relaxed voluntarily to the OFF state after turning off the power for a period of about 10 min, indicating the actually “volatile” nature of the ON state. Nevertheless, as observed from the fourth sweep (from 0 to 3 V) conducted over 10 min after turning off the power, the device exhibits essentially identical electrical OFF-to-ON switching behavior with the first sweep, and retains the high-conductivity state during the followed two sweeps (the fifth and the sixth sweeps), suggesting the “reprogrammable” characteristics of the current memory device. The seventh sweep was conducted about 10 min after turning off the power. The device was found to be also able to switch from the OFF state to the ON state when a reverse threshold voltage at around -1.8 V was applied. And the device remained in the ON state when the negative sweep (the eighth sweep) and the positive sweep (the ninth sweep) were repeated. The results observed here suggest that the current polyimide memory device can be written bi-directionally with almost no polarity at positive and negative threshold voltages of comparable magnitude. The tenth sweep was carried out about 10 min after turning off the power. The memory device was found to have relaxed voluntarily to the OFF state without any “erasing” process, whereas it could be reprogrammed to the ON

state when the threshold voltage at about -1.8 V was reapplied. Besides, the volatile ON state could be permanently retained by applying a refreshing voltage pulse of -1 V (1 ms duration) in every 5 s (the “rf” trace in Fig. 2(a)) or a continuous bias of -1 V (Fig. 2(c)).

The volatile, but reprogrammable nature of the ON state, and the bi-directionally accessible ON and OFF states observed above suggest that the current Au/Thin 6F/CzTPA PI layer/ITO sandwich device possesses electrical bistable characteristics that could serve as a static random access memory (SRAM) in digital information storage [37]. The OFF-to-ON electrical switching process is equivalent to the “writing” process in a traditional memory cell. The distinct and bi-directionally accessible bistable electrical states in the positive voltage range from 0 to 1.5 V and in the negative voltage range from 0 to -1.8 V allow any convenient voltage between 0 and 1.5 V or between 0 to -1.8 V (e.g. 1 V or -1 V) to “read” the “OFF” or “0” signal (before switching on) and the “ON” or “1” signal (after switching on) of the memory device in any order. The I – V characteristics of the device are demonstrated to have good reproducibility during repeated tests. And, further experiments on duplicated sandwich devices revealed that the observed electrical switching effect was repeatable, but with minor variations in the OFF-to-ON transition voltage. To this point, it is concluded that the synthesized 6F/CzTPA polyimide possesses unerasable but volatile, yet reprogrammable, bi-directionally accessible and nonpolar electrical bistabilities and the sandwich devices using the polyimide as the active layer could be applied as volatile SRAM memory in digital information storage. The low OFF-to-ON electrical transition voltage will endow the prepared SRAM devices with low power-consuming characteristic. However, it should be mentioned that, at a bias exceeding -5 V or $+5$ V, the device shows a sudden drop in the current to zero and could not be operated any more, which is suggested to be due to device failure at high electric field stress.

In addition to the SRAM memory effect and switching voltage, there are also many other important parameters that play crucial roles in determining the performance of a memory device and its eventual practical applications, including the ON/OFF current ratio, long-term retention stability, reading cycles and switching time. Fig. 2(b) shows the ON/OFF current ratio of the memory device as a function of the applied voltage. The results suggest that the sandwich device based on the 6F/CzTPA PI achieves an ON/OFF current ratio as high as around 10^5 during both the positive and negative switching-on process. The high ON/OFF current ratio achieved here promises a low misreading rate for the present devices during real memory applications. Furthermore, to evaluate the ability of the 6F/CzTPA polyimide in retaining the two conductivity states, the ON and OFF currents of the sandwich device were tested under ambient air conditions, the results of which are shown in Fig. 2(c). Under a constant bias stress of -1 V, the device shows excellent long-term operation stability and no degradation in current was observed for both the ON and OFF states over an 8 h period of measurement, demonstrating the excellent stability of the polyimide material and the observed electrical memory effect. And, it is expected that, with proper electronic encapsulation in practical applications, the retention time and the stability of the device will be promoted further or at least be retained intact. Fig. 2(d) shows the stimulus effect of the read pluses (-1 V in magnitude, 2 μ s in period, 1 μ s in duration width) on the ON and OFF states of the device. The result indicates no current degradation for both the ON and OFF states after more than 10^8 read cycles under continuous read pulses of -1 V, revealing the excellent information storage and reading out stabilities of the current memory device.

Another key performance indicator for a memory device is the switching time. Fig. 3 shows the transition response behavior of the memory device below and above the switching-on threshold voltage (i.e., 1.5 V as shown in Fig. 2(a)). The tested device was verified to be in an initial OFF state, and a read pulse with magnitude of 1 V (below the threshold voltage) could not switch it to the ON state, as shown in Fig. 3(a). Whereas, the device was immediately turned on when a read pulse of 2 V (above the threshold voltage) was applied, as shown in Fig. 3(b). And no distinguishable electrical delay was detected in Fig. 3b(b) within the resolution of the Keithley 4200 (upper limit of the pulse rising time: 20 ns). Thus, the switching time (i.e., response time, delay time) for the device is supposed to be in the nanoseconds scale and could be further confined to be faster than 20 ns. In addition to the ultrafast

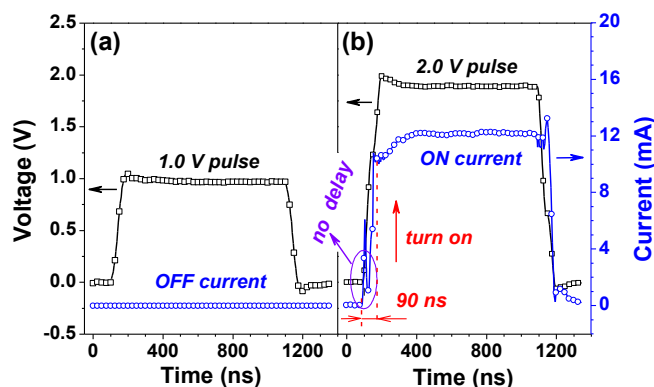


Fig. 3. The transient response of the device current vs. time below and above the switching-on threshold voltage. (a) The electrical current response of the device initially in the OFF state. A voltage pulse (1.0 V) less than the switching-on threshold voltage (1.5 V) is applied to confirm the low conductivity state of the device. (b) The electrical current response of the same device under a voltage pulse (2.0 V) higher than the switching-on threshold voltage. The device responds to the applied voltage immediately with no distinguishable electrical delay and is transformed to its equilibrium high conductivity state in ca. 90 ns.

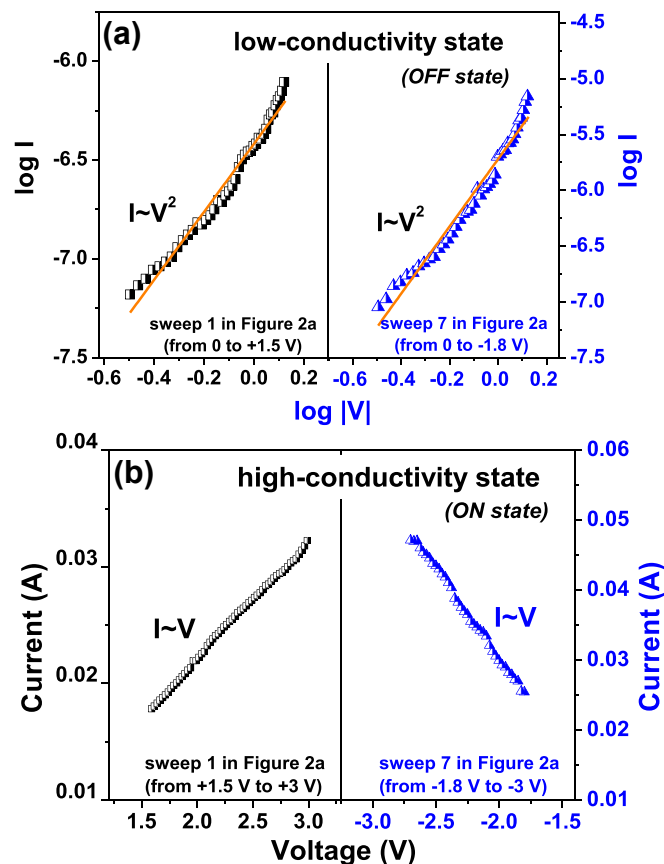


Fig. 4. (a) I – V characteristics fitted with the SCLC conduction model ($\log I \sim \log |V|$) for the memory device on the low-conductivity state (the OFF state) for both the positive sweep ($0 \rightarrow +1.5$ V) and the negative sweep ($0 \rightarrow -1.8$ V). (b) I – V characteristics fitted with the Ohmic conduction model ($I \sim V$) for the memory device on the high-conductivity state (the ON state) for both the positive sweep ($+1.5 \rightarrow +3.0$ V) and the negative sweep ($-1.8 \rightarrow -3.0$ V).

response time, the result in Fig. 3(b) also indicates that the device soon reaches its equilibrium ON state from the initial OFF state in a period as short as ca. 90 ns. Here, it should be mentioned that both the response time and the equilibrium time of the current memory device are much faster than that (~ 1 μ s) of a NAND (NOT/AND) flash memory based on traditional semiconductors, and comparable to the current widely-used dynamic random access memory (DRAM) and SRAM inorganic semiconducting memory devices (response time: <10 ns, access time: 60 – 100 ns or shorter) [14,51,52]. On account of the above results, it is suggested that the present polyimide constitutes a considerably promising candidate material for the next-generation digital memory applications with characteristics of mass storage capacity and ultrafast data access. The ultrafast response time and the short equilibrium time will ensure the fabricated memory device with the lowest misoperation and the highest accuracy during the ultrafast read/write process. In addition, as a further consideration, the fast switching-on behavior observed in the current memory device implies that the charge transfer occurring in the 6F/CzTPA donor–acceptor polyimide system is considerably rapid under the applied electric field.

3.3. Theoretical analysis, molecular simulation and switching mechanism

3.3.1. Theoretical analysis

Many physical models have been proposed to explain the current transition in a dielectric film, including Ohmic conduction,

Hopping conduction, Schottky emission, thermionic emission (TE), Frenkel–Poole emission, tunnel or field emission, direct tunneling, Fowler–Nordheim tunneling, ionic conduction, and space-charge-limited current (SCLC) transport [2,9,53]. However, for the present case, it is found that any individual conduction mechanism mentioned above cannot fit the characteristics for both the ON state and the OFF state at the same time, implying the involvement of probably different charge transport processes in the two accessible states. Fig. 4(a) shows the I – V characteristics of the memory devices in OFF states, presenting in the form of $\log I$ vs. $\log |V|$. As can be observed, during both the positive sweep (sweep 1 in Fig. 2(a), $0 \rightarrow +1.5$ V) and the negative sweep (sweep 7 in Fig. 2(a), $0 \rightarrow -1.8$ V), the low conduction states have well been characterized by the space-charge-limited current (SCLC) model in which $\log I$ is linearly proportional to $\log |V|$ ($\log I \sim \log |V|$). The power law of the I – V result observed here suggests that the memory device undergoes a restricted carrier injection and transportation process at the initial stage of the voltage scan. And it is reasonable to deduce that, when the applied bias exceeds the threshold value, numerous charges will be generated and injected into the polyimide active layer, and the ultrafast charge-transfer process (as elicited in Fig. 3) will soon yield a conducting path with the fastest speed, triggering the device to its high conduction state. The basically linearly-correlated I – V characteristics shown in Fig. 4(b) for the ON states of the device suggest that the high conductivity state is well fitted to the Ohmic conduction relationship ($I \sim V$) in the range of $+1.5$ V \rightarrow $+3.0$ V (sweep 1 in Fig. 2(a)) and -1.8 V \rightarrow -3.0 V (sweep 7 in Fig. 2(a)), indicating that the charge carriers in the polyimide active layer overcome the SCLC energy barriers and eventually flow through the device by the Ohmic conduction processes at the higher biases during both the positive and negative voltage sweeps. The laws of the charge transport by the SCLC and Ohmic models are given by the following equations.

$$J_{\text{SCLC}} \propto \frac{9\epsilon_i \mu V^2}{8d^3} \quad (3)$$

$$J_{\text{Ohmic}} \propto V \exp \frac{-\Delta E_{\text{ae}}}{kT} \quad (4)$$

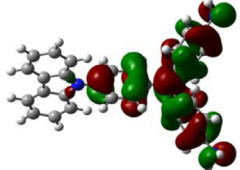
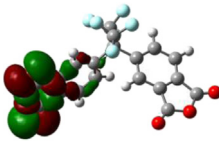
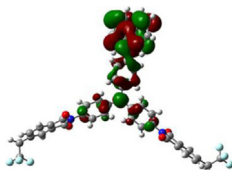
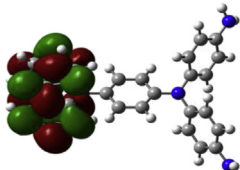
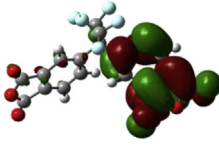
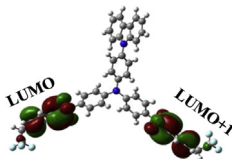
(J = current density, V = electric field, T = temperature, ϵ = insulator dynamic permittivity, d = insulator thickness, q is charge, and μ is the carrier mobility.) [9].

3.3.2. Molecular simulation

With the purpose of getting a clear understanding of the charge transfer process and the corresponding switching behavior of the present polyimide memory device, molecular simulations were carried out to elucidate the electronic structures, molecular orbitals, energy levels and dipole moments of our synthesized electroactive donor–acceptor macromolecules. For the sake of model simplicity and practical availability for computations, 4,4'-dipthalimido-4''-N-carbazolyltriphenylamine, with one DACzTPA tethered via imide rings to two 6FDA fragments (see Table 1 for model compound **1**), which is essentially identical to the basic unit of the 6F/CzTPA polyimide were selected as the model compound. Different calculation methods ranging from semi-empirical (including AM1 and PM3) to ab initio (including HF) and density functional theory (including LSDA, B3LYP, and B3PW91) were evaluated. The basis set was set as 6-31G(d), whenever necessary, in all the first-principle calculations.

Fig. 5 summarized the calculated HOMO and LUMO energy levels, and the related energy band gaps obtained from the molecular simulations conducted on different theory levels. To verify the reliability of the simulation results, the corresponding experimental HOMO, LUMO and band gap results determined from the UV/vis absorption spectrum and the CV sweeps of the 6F/CzTPA polyimide (see Fig. 1) were also shown. The results indicate that the worst results come from the semi-empirical-based computations (AM1 and PM3) and the ab initio (HF) calculations, with the observation of considerably large deviations from the experimental results either in energy levels or in energy band gaps, indicating their unavailability in predicting the electronic structures of the

Table 1
Molecular simulation results for the components in 6F/CzTPA PI based on B3LYP/6-31G(d) model chemistry.^{a,b}

Components	DACzTPA	6FDA	Model compound 1
HOMO level	 (-4.76 eV)	 (-8.20 eV)	 (-5.28 eV)
LUMO level	 (-0.31 eV)	 (-2.27 eV)	 (-2.21 eV)
Energy gap	4.45 eV	5.33 eV	3.07 eV
Dipole moment	4.304 Debye	5.223 Debye	3.990 Debye

^a All the structures used for molecular orbital calculations were optimized firstly on AM1 level and then on HF/6-31G(d) level.

^b The structure of the 6F/CzTPA model compound **1** was constructed from the optimized 6FDA and CzTPA structure, and then optimized additionally on AM1 and HF/6-31G(d) level.

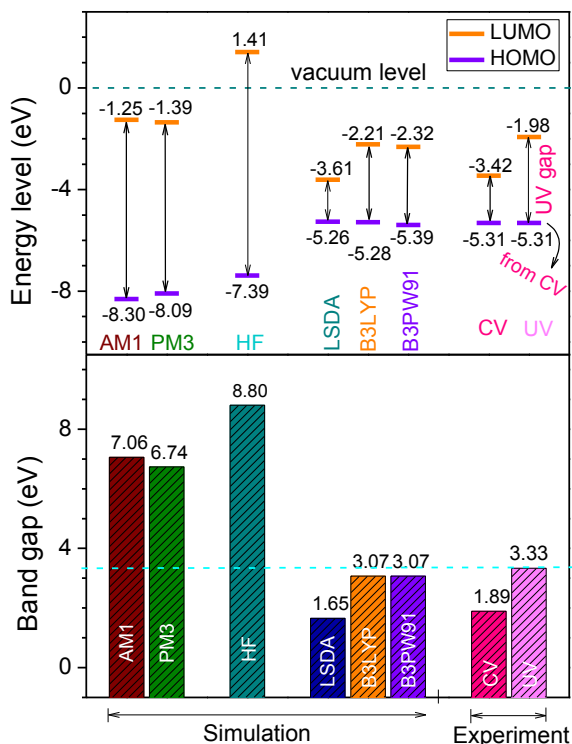


Fig. 5. Comparison of the energy band gaps (bottom) and the HOMO, LUMO energy levels (top) of the 6F/CzTPA model compound **1** calculated from model chemistry on different theory levels and those determined from the cyclic voltammetry (CV) and UV/vis absorption spectrum of the polyimide. The basis set of 6-31G(d) was used in the ab initio and DFT calculations.

current polyimide. DFT methods, especially B3LYP and B3PW91, exhibit the best accuracy, in which the calculations based on the B3LYP/6-31G(d) theory level gave the most acceptable results. The HOMO, LUMO, and band gaps calculated from the B3LYP/6-31G(d) model chemistry are -5.28 eV, -2.21 eV, and 3.07 eV, respectively, which are almost identical with the experimentally-determined results, -5.31 eV, -1.98 eV, and 3.33 eV. Therefore, the B3LYP/6-31G(d) model chemistry was eventually selected for all future simulations and discussions.

Table 1 shows the corresponding B3LYP/6-31G(d)-based simulation results for the DACzTPA unit, the 6FDA unit, and the model compound **1** used to represent the 6F/CzTPA polyimide. The higher HOMO energy level of DACzTPA (-4.76 eV) indicates that the DACzTPA unit consisted of triphenylamine and carbazole groups functions as the hole-accepting moieties (electron donor), while the lower LUMO energy level of 6FDA (-2.27 eV) indicates the strong electron-withdrawing ability of the 6FDA unit and its availability to function as electron acceptor. The HOMO and LUMO energy levels of the model compound **1** (representative of the polyimide) are -5.28 eV and -2.21 eV, respectively, which are basically consistent with the results obtained from the CV and UV/vis spectra of the polyimide. These results indicate that when these two components are covalently connected, the HOMO of the 6F/CzTPA unit is located on the DACzTPA side with a decreased HOMO energy level, whereas the LUMO of the 6F/CzTPA unit is located on the 6FDA side with an increased LUMO energy level. The 6F/CzTPA polyimide system is supposed to possess similar electronic structures, with DACzTPA functioning as the electron donor and 6FDA as the electron acceptor. The two 6FDA fragments attached with the DACzTPA unit are supposed to serve as two effective electron-trapping sites since they correspond to the LUMO and LUMO + 1

orbitals, respectively, as illustrated in Table 1. The tethering of Cz to TPA and the subsequent formation of the DACzTPA moieties are supposed to significantly enhance the electron-donating characteristics of the resulting material since the results indicate that the HOMO, HOMO-1, HOMO-2, HOMO-3, HOMO-4 and HOMO-5 orbitals are all located on the CzTPA groups (see Fig. S5). Besides, the reduced dipole moment (3.990 Debye) observed for the model compound **1** in Table 1, as relative to the individual CzTPA (4.304 Debye) and 6FDA (5.223 Debye), suggests that the synthesized polyimide has a strong tendency for charge separation. These features promise easier charge transfer from DACzTPA (HOMOs) to 6FDA (LUMOs), and the subsequent formation of charge-transfer complexes in the polyimide system.

3.3.3. Switching mechanism

Fig. 6 shows the energy level diagram for the sandwich devices with the configuration of ITO/Thin 6F/CzTPA PI Layer/Au. The HOMO and LUMO energy levels of the polyimide determined from CV and UV/vis spectra are -5.31 eV and -1.98 eV, respectively, which are associated in respective with the DACzTPA moieties and the 6FDA units based on the quantum calculations. For the positive scan, ITO serves as the cathode and Au as the anode. It is clear in Fig. 6 that the electron-transfer energy barrier between the ITO electrode and the LUMO level of the 6F/CzTPA PI (2.82 eV) is considerably higher than that between the HOMO level of the 6F/CzTPA PI and the Au electrode (0.21 eV). While for the negative scan, ITO is the anode and Au is the cathode. Whereas, the electron-transfer energy barrier of the Au/6F/CzTPA LUMO (3.12 eV) is still higher than that of the 6F/CzTPA HOMO/ITO (0.51 eV), and both of which are larger than the energy barriers in the positive scan (i. e., 2.82 eV and 0.21 eV). In terms of these data, it is inferred that the 6F/CzTPA PI most likely functions as a p-type material and hole injection from metal electrodes into the HOMO of the polyimide is more favorable during the charge injection process.

Taking the positive scanning process ($0 \rightarrow +3.0$ V) as an example, theoretically speaking, an applied voltage exceeding 0.21 eV (the barrier between Au and the HOMO of the polyimide) will provide enough energy for the holes on Au (or electrons on HOMO) to overcome the energy barrier between Au and the HOMO to inject into (for electrons, extract from) the active layer of the sandwich device. Thus, during the voltage scanning process, holes are readily loaded into the material under a low bias. Accordingly, the device exhibits an instant increase in the current (although to merely $10^{-8} \sim 10^{-7}$ A scale) at the very initial stage of the voltage sweep, as observed in Fig. 2(a) (the first scan). However, it is

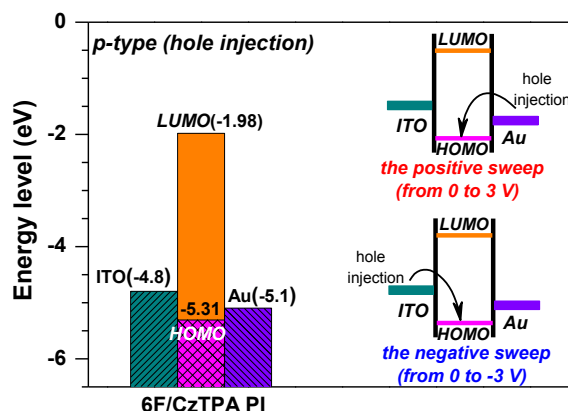


Fig. 6. Energy level diagram for the ITO/Thin 6F/CzTPA PI Layer/Au sandwich device.

supposed that hole injection (or electron extraction) under bias scans before switching on should be rather limited, as it has been verified in Fig. 4(a) that the I – V characteristics of the device in the low-conductivity state agree fairly well with the SCLC conduction model. This is reasonable and expected, since the CzTPA unit in the 6F/CzTPA polyimide bears a triphenylamine group in the polymer main chain and a carbazole unit as the pendent, both of which are typical and efficient electron-donating moieties, and correspondingly possess strong and definitely enhanced hole-trapping abilities when combining together. Besides, simulation results in Table 1 suggest that the 6FDA moieties will also exhibit significant effect in blocking the mobility of the injected holes, due to their considerably low HOMO energy level (-8.20 eV). As a result, charge carrier migration in the active layer, which is responsible for the electrical conductance of the device, is considerably limited. Concomitantly, the injected holes will induce a countering space-charge field in the polyimide matrix, which will screen the applied external electric field, thereby hampering further charge injection into the active layer [54]. Thus, the material exhibits a high-resistance state and follows the SCLC conduction process, accounting for the limited increase in the device current below 1.5 V.

With the increase of the applied external electric field, and the continuous injection of the holes into the HOMOs (HOMO, HOMO-1, HOMO-2, HOMO-3, HOMO-4, HOMO-5, see Fig. S5) located on the CzTPA moieties and the corresponding electron injection into the LUMOs (LUMO, LUMO + 1, LUMO + 2, LUMO + 3, see Fig. S5) located on the 6FDA parts, open channels for charge carriers were finally generated between the charged HOMOs and charged LUMOs through the charge-transfer interactions and the subsequent formation of charge-transfer (CT) complexes. Consequently, a progressive increase in current was observed and the memory device was suddenly triggered to its low-resistance state. The data-fitting results shown in Fig. 4(b) suggest that the I – V behaviors since switching on (i.e., after 1.5 V) have been well characterized by the Ohmic conduction model, manifesting the change of the conduction mechanisms in the ON state. The device further remains in its high-conductivity state during the subsequent positive and negative sweeps, which is suggested to be due to the strong electron affinity of the 6FDA units, which could effectively hold the electrons trapped in 6FDA moieties, and hamper their escapes through the formation of CT complexes. Besides, the decreased dipole moment (3.990 Debye) of the 6F/CzTPA basic unit, as compared to the individual 6FDA (5.223 Debye) and CzTPA (4.304 Debye) parts, as listed in Table 1, implies that it will also be able to help to promote the generation and the subsequent stabilization of the formed charge separation structures. Therefore, the polymer could not be reset to its initial OFF state during the followed bi-directional voltage scans and the device manifests “unerasable” characteristics in the ON state, as displayed in Fig. 2(a). However, the ON state is turned out to be actually “volatile”. Over 10 min after turning off the power, the device is automatically retrieved to the initial low-conductivity OFF state, yet is “reprogrammable”. This indicates that the CT complexes formed during the charge injection processes are actually “temporarily stable” and “reversible”, which might be partially verified by an indirect but explicit experimental evidence, i.e., the quasi-reversible oxidation and reduction behaviors observed in the CV test cycles depicted in Fig. 1(b). Mechanistically, it is deduced that, although both the strong electron-withdrawing ability of the 6FDA part and the decreased dipole moment of the 6F/CzTPA basic unit have positive effects in stabilizing the formed CT complexes and in helping retaining the trapped electrons through the increase of the back-charge-transfer energy barriers, they could not inhibit their escapes and further neutralization with the holes trapped at the CzTPA species in the polyimides, due to the

strong electron-withdrawing abilities of the CzTPA unit after hole trapping and the important but easy-to-be-neglected fact that the charge-trapping sites located on CzTPA are stoichiometrically excess as compared to 6FDA (see Fig. S5). As a result, the device shows a volatile SRAM memory effect.

The device is supposed to obey the same conduction mechanism when starting with a negative voltage sweep process ($0 \rightarrow -3.0$ V). The slightly higher switching-on threshold voltage (i.e., -1.8 V) observed during the negative sweep is suggested to be related to the relatively higher energy barriers encountered during the negative sweep (i.e., 0.51/3.12 eV vs. 2.82/0.21 eV), as depicted in Fig. 6.

4. Conclusions

In summary, an electrical resistive switching volatile static random access memory (SRAM) behavior was realized in our present work, based on an aromatic polyimide, 4,4'-(hexafluoroisopropylidene)diphthalic anhydride/4,4'-(hexafluoroisopropylidene)diphenylamine (6F/CzTPA PI), with structures in which the carbazole-tethered triphenylamine units (CzTPA) function as the electron-donating moieties and the hexafluoroisopropylidene phthalimide units (6FDA) serve as the electron-accepting species. The fabricated memory device in a simple ITO/polyimide/Au sandwich structure exhibits two bi-directionally accessible conductivity states during both the positive and negative voltage sweeping processes with the achievement of an ON/OFF current ratio as high as about 10^5 , and displays no polarity except for a trivial variation in the switching voltage. The device exhibits rather fast response speed with a switching time less than 20 ns. Moreover, both the ON and OFF states were stable under a constant voltage stress of -1 V and survived up to 10^8 read cycles with a -1 V periodic read pulse. The I – V characteristic of the device on the OFF state agrees fairly well with the space-charge-limited current (SCLC) model, while it turns to the Ohmic conduction model on the ON state. The roles of the donor and acceptor components in the memory mechanism of the electroactive polyimide were elucidated via molecular simulation. The strong electron-donating ability of the carbazole-tethered triphenylamine moieties and their stoichiometrically excess charge-trapping sites as compared to the 6FDA units are suggested to play an important role in realizing the temporarily unerasable, but eventually volatile SRAM memory effect observed in the current system.

Acknowledgments

The authors thank the financial support from the National Key Basic Research Program of China (973 Program, project No. 2014CB643600), Fundamental Research Funds for the Central Universities of China (project No. ZZ1306), National Natural Science Foundation of China (project No. 50903006), the Specialized Research Fund for the Doctoral Program of Higher Education (project No. 20090010120008), and the Program for SCI@guoshi of CETV.

Appendix A. Supplementary material

Supplementary material related to this article can be found online at <http://dx.doi.org/10.1016/j.polymer.2013.12.046>.

References

- [1] Rath AK, Dhara K, Banerjee P, Pal AJ. *Langmuir* 2008;24:5937–41.
- [2] Bandyopadhyay A, Pal AJ. *Adv Mater* 2003;15:1949–52.
- [3] Stikeman A. *Technol Rev* 2002;105:31.
- [4] Möller S, Perlov C, Jackson W, Taussig C, Forrest SR. *Nature* 2003;426:166–9.
- [5] Hahm SG, Choi S, Hong SH, Lee TJ, Park S, Kim DM, et al. *Adv Funct Mater* 2008;18:3276–82.

- [6] Wang KL, Liu YL, Lee JW, Neoh KG, Kang ET. *Macromolecules* 2010;43:7159–64.
- [7] You NH, Chueh CC, Liu CL, Ueda M, Chen WC. *Macromolecules* 2009;42:4456–63.
- [8] Yang Y, Ouyang J, Ma L, Tseng RJH, Chu CW. *Adv Funct Mater* 2006;16:1001–14.
- [9] Ling QD, Liaw DJ, Zhu C, Chan DSH, Kang ET, Neoh KG. *Prog Polym Sci* 2008;33:917–78.
- [10] Pradhan B, Das S. *Chem Mater* 2008;20:1209–11.
- [11] Ling QD, Kang ET, Neoh KG, Chen Y, Zhuang XD, Zhu C, et al. *Appl Phys Lett* 2008;92:143302.
- [12] Lai YS, Tu CH, Kwong DL, Chen JS. *Appl Phys Lett* 2005;87:122101.
- [13] Lai YS, Tu CH, Dim-Lee K, Chen JS. *IEEE Electron Device Lett* 2006;27:451–3.
- [14] Ling QD, Wang W, Song Y, Zhu CX, Chan DSH, Kang ET, et al. *J Phys Chem B* 2006;110:23995–4001.
- [15] Teo EYH, Ling QD, Song Y, Tan YP, Wang W, Kang ET, et al. *Org Electron* 2006;7:173–80.
- [16] Tian GF, Qi SL, Chen F, Shi L, Hu WP, Wu DZ. *Appl Phys Lett* 2011;98:203302.
- [17] Wang KL, Tseng TY, Tsai HL, Wu SC. *J Polym Sci Part A Polym Chem* 2008;46:6861–71.
- [18] Park S, Kim K, Kim JC, Kwon W, Kim DM, Ree M. *Polymer* 2011;52:2170–9.
- [19] Li Y, Chu Y, Fang R, Ding S, Wang Y, Shen Y, et al. *Polymer* 2012;53:229–40.
- [20] Tian GF, Wu DZ, Shi L, Qi SL, Wu ZP. *RSC Adv* 2012;2:9846–50.
- [21] Tseng RJ, Huang J, Ouyang J, Kaner RB, Yang. *Nano Lett* 2005;5:1077–80.
- [22] Lai Q, Zhu Z, Chen Y, Patil S, Wudl F. *Appl Phys Lett* 2006;88:133515.
- [23] Qi SL, Iida H, Liu L, Irle S, Hu W, Yashima E. *Angew Chem Int Ed* 2013;52:1049–53.
- [24] Paul S, Kanwal A, Chhowalla M. *Nanotechnology* 2006;17:145–51.
- [25] Ling QD, Lim SL, Song Y, Zhu CX, Chan DSH, Kang ET, et al. *Langmuir* 2007;23:312–9.
- [26] Liu G, Ling QD, Teo EYH, Zhu CX, Chan DSH, Neoh KG, et al. *ACS Nano* 2009;3:1929–37.
- [27] Hwang SK, Lee JM, Kim S, Park JS, Park HI, Ahn CW, et al. *Nano Lett* 2012;12:2217–21.
- [28] Son DI, Kim TW, Shim JH, Jung JH, Lee DU, Lee JM, et al. *Nano Lett* 2010;10:2441–7.
- [29] Zhuang XD, Chen Y, Liu G, Li PP, Zhu CX, Kang ET, et al. *Adv Mater* 2010;22:1731–5.
- [30] Ling QD, Liaw DJ, Teo EYH, Zhu C, Chan DSH, Kang ET, et al. *Polymer* 2007;48:5182–201.
- [31] Kim K, Park S, Suk GH, Lee TJ, Kim DM, Kim JC, et al. *J Phys Chem B* 2009;113:9143–50.
- [32] Kim DM, Park S, Lee TJ, Hahm SG, Kim K, Kim JC, et al. *Langmuir* 2009;25:11713–9.
- [33] Chen CJ, Yen HJ, Chen WC, Liou GS. *J Mater Chem* 2012;22:14085–93.
- [34] Lee TJ, Park S, Hahm SG, Kim DM, Kim K, Kim J, et al. *J Phys Chem C* 2009;113:3855–61.
- [35] Fang YK, Liu CL, Yang GY, Chen PC, Chen WC. *Macromolecules* 2011;44:2604–12.
- [36] Kuurosawa T, Chueh CC, Liu CL, Higashihara T, Ueda M, Chen WC. *Macromolecules* 2010;43:1236–44.
- [37] Liu YL, Wang KL, Huang GS, Zhu CX, Tok ES, Neoh KG, et al. *Chem Mater* 2009;21:3391–9.
- [38] Kim K, Yen HJ, Ko YG, Chang CW, Kwon W, Liou GS, et al. *Polymer* 2012;53:4135–44.
- [39] Yu AD, Kuurosawa T, Lai YC, Higashihara T, Ueda M, Liu CL, et al. *J Mater Chem* 2012;22:20754–63.
- [40] Liu CL, Kuurosawa T, Yu AD, Higashihara T, Ueda M, Chen WC. *J Phys Chem C* 2011;115:5930–9.
- [41] Ling QD, Chang FC, Song Y, Zhu CX, Liaw DJ, Chan DSH, et al. *J Am Chem Soc* 2006;128:8732–3.
- [42] Tian GF, Wu DZ, Qi SL, Wu ZP, Wang XD. *Macromol Rapid Commun* 2011;32:384–9.
- [43] Hsu JC, Chen Y, Kakuchi T, Chen WC. *Macromolecules* 2011;44:5168–77.
- [44] Ko YG, Kwon W, Yen HJ, Chang CW, Kim DM, Kim K, et al. *Macromolecules* 2012;45:3749–58.
- [45] Yen HJ, Chen CJ, Liou GS. *Adv Funct Mater* 2013. <http://dx.doi.org/10.1002/adfm.201300569>.
- [46] Kim DM, Ko YG, Choi JK, Kim K, Kwon W, Jung J, et al. *Polymer* 2012;53:1703–10.
- [47] Chen YC, Huang GS, Hsiao CC, Chen SA. *J Am Chem Soc* 2006;128:8549–58.
- [48] Chen F, Tian GF, Shi L, Qi SL, Wu DZ. *RSC Adv* 2012;2:12879–85.
- [49] Djurovich PI, Mayo EI, Forrest SR, Thompson ME. *Org Electron* 2009;10:515–20.
- [50] Lee YZ, Chen X, Chen SA, Wei PK, Fann WS. *J Am Chem Soc* 2001;123:2296–307.
- [51] Ma LP, Liu J, Yang Y. *Appl Phys Lett* 2002;80:2997–9.
- [52] Kanwal A, Paul S, Chhowalla M. *Mater Res Soc* 2005;830:D7.2.1–7.2.5.
- [53] Ling QD, Song Y, Lim SL, Teo EYH, Tan YP, Zhu C, et al. *Angew Chem Int Ed* 2006;45:2947–51.
- [54] Liu G, Ling QD, Kang ET, Neoh KG, Liaw DJ, Chang FC, et al. *J Appl Phys* 2007;102. 024502.